Accepted Manuscript
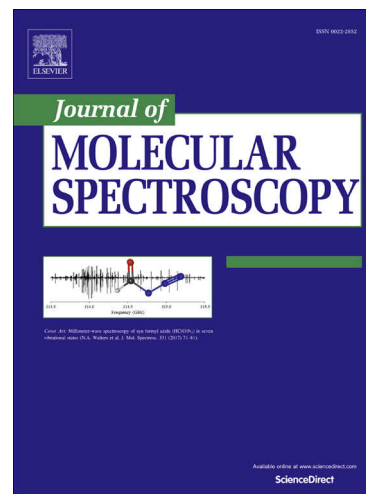
Nonresonant Raman spectra of the methyl radical $^{12}CH_3$ simulated in variational calculations

Ahmad Y. Adam, Per Jensen, Andrey Yachmenev, Sergei N. Yurchenko

Nonresonant Raman spectra of the methyl radical $^{12}CH_3$ simulated in variational calculations

Ahmad Y. Adam[a], Per Jensen[a], Andrey Yachmenev[b], Sergei N. Yurchenko[c]

[a]*Physikalische und Theoretische Chemie, Fakultät für Mathematik und Naturwissenschaften, Bergische Universität Wuppertal, D-42097 Wuppertal, Germany*
[b]*Center for Free-Electron Laser Science, Deutsches Elektronen-Synchrotron DESY, Notkestraße 85, D-22607 Hamburg, Germany and Hamburg Center for Ultrafast Imaging, Universität Hamburg, Luruper Chaussee 149, D-22761 Hamburg, Germany*
[c]*Department of Physics and Astronomy, University College London, Gower Street, London WC1E 6BT, United Kingdom*

Abstract

We report first-principles variational simulation of the non-resonant Raman spectrum for methyl radical ($^{12}CH_3$) in the electronic ground state. Calculations are based on a high level *ab initio* potential energy and polarizability tensor surfaces of CH_3 and employ the accurate variational treatment of the ro-vibrational dynamics implemented in the general code TROVE [S. N. Yurchenko, W. Thiel, and P. Jensen, *J. Mol. Spectrosc.* **245**, 126–140 (2007); A. Yachmenev and S. N. Yurchenko, *J. Chem. Phys.* **143**, 014105 (2015)]. TROVE can be applied to arbitrary molecules of moderate size and we extend here its capabilities towards simulations of Raman spectra. The simulations for CH_3 are found to be in a good agreement with the available experimental data.

Keywords: Raman spectra, simulation, variational calculations, methyl radical, CH_3.

1. Introduction

In a recent publication [1] we reported the computation, by variational methods, of a so-called line list, i.e., a catalogue of absorption lines, valid up to temperatures of 1500 K for the methyl radical CH_3 in the electronic ground state. The computations were based on high level *ab initio* potential energy and polarizability tensor surfaces. In addition, we have previously studied theoretically the hyperfine coupling constant (HFCC) of CH_3 isotopologues [2], confirming previous results that for this radical, vibrational motion must be considered in order that accurate HFCC values be obtained.

As explained in Ref. [1] (to which the reader is referred for details and references), the methyl radical is important in combustion processes and as an intermediate in many chemical reactions of industrial and/or environmental interest. Also, it has been observed in interstellar space and in planetary atmospheres.

Experimental observations of CH_3 are most often done in absorption or emission. Owing to the importance of CH_3 in diverse areas it is of interest to use observed spectra to determine its concentrations or column densities in remote environments such as interstellar space. For obtaining concentrations or column densities from observed intensities, however, the transition moments of the observed transitions must be known (see, for example, Ref. [3]). In order to measure the transition moments in the laboratory, one must prepare a sample of molecules at a known concentration. This is in itself difficult in the case of unstable, short-lived molecules such as CH_3 (and it is also difficult

to reach concentrations large enough for detection), and so the concentration determinations often rely on theoretical predictions of the transition moments [4, 5]. The ExoMol project by Yurchenko, Tennyson and co-workers [6, 7] aims at providing theoretically computed transition moments and simulated spectra for (small to medium-sized) general polyatomic molecules of astrophysical and/or -chemical interest.

The remote-sensing tools used for probing environments such as interstellar space, atmospheres of the Earth and exoplanets, the outer layers of cool stars, etc., are absorption or emission spectra with intensities generated by the molecular electric dipole moment operator. Thus, work aimed at facilitating the interpretation of remote-sensing spectra, such as that carried out in the ExoMol project [6, 7], is focused on absorption and emission spectroscopy. However, the corresponding molecular transitions are subject to fairly restrictive selection rules (see, for example, Chapter 14 of of Ref. [8]). To obtain spectra with a larger selection of transitions, one can change the experimental method. Raman spectroscopy (see, for example, Section 14.3 of of Ref. [8]) is an example of a spectroscopic technique with selection rules less restrictive than those of absorption and emission spectroscopy [9]. It is illusory, however, to imagine the observation of remote-sensing Raman spectra of, say, interstellar space; the Raman spectra are much too weak for that. The theoretical prediction of transition probabilities for Raman transitions, analogous to the theoretical calculations of transition moments for absorption and emission, assists the determination of molecular concentrations from Raman spectra recorded in the laboratory. An example of astrophysically interesting molecules being characterized by Raman spectra is the recent work on dimethyl ether by Fernández *et al.* [10].

The development of electronic-structure and nuclear-motion

---

*Corresponding author Tel: +49 202 439 2468; Fax: +49 202 439 2505
Email address:* `jensen@uni-wuppertal.de` (Per Jensen)

methods for computing Raman intensities is an active area of research, not only for gas phase spectra [11], but also for investigating new phenomena like hyper-Raman scattering [12, 13], characterizing new crystalline materials [14] and understanding surface-enhanced Raman scattering [15].

In 1928, the Raman effect was discovered in liquids by Raman and his student Krishnan [16] and, independently, in crystals by Landsberg and Mandelstam [17]. The effect had been predicted theoretically by Smekal in 1923 [18]. A more recent development of 'standard' Raman spectroscopy (also called *nonresonant Raman spectroscopy*) is the *resonance Raman* (RR) technique [19, 20, 21, 22, 23]. An RR experiment makes use of a frequency-tunable laser for producing the incident radiation, whose frequency is selected to coincide with an electronic transition of the molecule. This leads to a dramatic increase of the Raman intensity and a corresponding decrease in the molecular concentrations detectable in Raman experiments. Another advantage of RR experiments is that it is possible to select to enhance the intensity of transitions to a particular vibrational level of the molecule.

The existing computational procedures for simulating nonresonant Raman spectra, in particular those implemented in electronic-structure (*ab initio*) programs, neglect rotational motion and treat the vibronic motion in the so-called double-harmonic approximation. In this approximation, the potential energy function is harmonic, i.e., it is represented as a second-order Taylor expansion in the vibrational coordinates, and the analogous expansions of the polarizability tensor elements are truncated after the linear terms. Present-day simulations of absorption and emission spectra, however, are made in an approximation highly superior to the double-harmonic one, taking into account rotation and employing 'fully coupled', variationally determined rovibronic wavefunctions, and the corresponding rovibronic energies, for computing the spectra. For example, in much of the absorption/emission simulation work carried out within the ExoMol project, high-level, variationally computed rovibronic wavefunctions from the TROVE [24, 25] program are used. In the present work, we develop a theoretical approach to simulate nonresonant Raman spectra in terms of rovibronic wavefunctions from TROVE [24, 25]. With the resulting computational procedure, we are able to simulate nonresonant Raman spectra in the same high-level approximation currently routinely employed for absorption and emission spectra. Developments of the traditional, nonresonant Raman-spectroscopy technique, such as the resonance Raman [19, 20, 21, 22, 23] and hyper-Raman scattering [12, 13] techniques mentioned above, together with coherent anti-Stokes Raman (CARS) spectroscopy [26], and coherent Raman photofragment spectroscopy [27], have higher sensitivity than the traditional Raman method, and the present work can be seen as a first step towards the development of theoretical methods to simulate the corresponding spectra.

We have employed the newly developed theoretical approach for simulating the nonresonant Raman spectrum of CH_3. For this radical, the three fundamental bands ν_1, ν_3, and ν_4 are observable by Raman spectroscopy; ν_1 is only observable as Raman transition, whereas ν_3 and ν_4 are also observable in absorption and emission. The calculations of the present work are based on high-level *ab initio* potential energy and polarizability surfaces.

2. Theory and computational details

2.1. Potential energy surface

For this work we employ a high level *ab initio* potential energy surface (PES) of CH_3 from Ref. [2], computed using the partially spin-restricted open-shell explicitly correlated coupled cluster theory RCCSD(T)-F12b [28] in conjunction with the F12-optimized correlation consistent valence basis set cc-pVQZ-F12 [29]. The PES is represented by a Taylor series expansion around equilibrium geometry in terms of the symmetry-adapted combinations of valence bond coordinates [30].

2.2. Polarizability surfaces

The electronically averaged polarizability surfaces for CH_3 were computed using the MOLPRO [31] program package. Frozen-core calculations were carried out for 19 361 symmetry-unique geometries using the spin-restricted open-shell coupled cluster theory RCCSD(T) [32] and the augmented correlation consistent valence basis set aug-cc-pVTZ [33, 34], employing the three-point stencil finite difference formula for the second derivative with the electric field strength of 0.002 a.u.

To represent the electronically averaged polarizability surfaces analytically, we use a representation analogous to the so-called symmetry-adapted molecular bond (SMB) representation described for the dipole moment in Ref. [35]. For a molecule with $\boldsymbol{D}_{3h}(M)$ (see Table A-10 of Ref. [8]) symmetry, the SMB dipole moment is described in terms of symmetrized projections of the dipole moment vector onto the normalized molecular bond vectors

$$\mathbf{e}_j = \frac{\mathbf{r}_j - \mathbf{r}_4}{|\mathbf{r}_j - \mathbf{r}_4|}, \quad j = 1, 2, 3, \tag{1}$$

where $\mathbf{r}_j$ is the position vector of proton j in the molecule-fixed axis system *xyz*, and $\mathbf{r}_4$ is the position vector of the C nucleus. The vectors $\mathbf{e}_j$ are understood as row (1×3) matrices.

For the components of the polarizability tensor, we introduce analogous, analytical SMB functions by following the procedure presented in Refs. [35, 36, 37, 38]. The polarizability tensor for a molecule with $\boldsymbol{D}_{3h}(M)$ symmetry spans the reducible representation $2A'_1 \oplus E' \oplus E''$ and functions generating

the individual irreducible representations are given as

$$\bar{\alpha}_{A_1'}^{(1)} = \frac{1}{\sqrt{3}}(\bar{\alpha}_{11} + \bar{\alpha}_{22} + \bar{\alpha}_{33}), \tag{2}$$

$$\bar{\alpha}_{E_a'}^{(2a)} = \frac{1}{\sqrt{6}}(\bar{\alpha}_{12} - \bar{\alpha}_{13} - \bar{\alpha}_{23}), \tag{3}$$

$$\bar{\alpha}_{E_b'}^{(2b)} = \frac{1}{\sqrt{2}}(\bar{\alpha}_{13} - \bar{\alpha}_{23}), \tag{4}$$

$$\bar{\alpha}_{A_1'}^{(3)} = \bar{\alpha}_{44}, \tag{5}$$

$$\bar{\alpha}_{E_a''}^{(4a)} = \frac{1}{\sqrt{6}}(2\bar{\alpha}_{14} - \bar{\alpha}_{24} - \bar{\alpha}_{34}), \tag{6}$$

$$\bar{\alpha}_{E_b''}^{(4b)} = \frac{1}{\sqrt{2}}(\bar{\alpha}_{24} - \bar{\alpha}_{34}), \tag{7}$$

where

$$\bar{\alpha}_{ij} = \mathbf{e}_i \cdot \left(\bar{\alpha} \, \mathbf{e}_j^{\mathrm{T}} \right), \quad i, j = 1, 2, 3, 4 \tag{8}$$

(with a superscript T denoting transposition) are projections of the 3×3 electronically averaged polarizability tensor $\bar{\alpha}$ onto the molecular bond vectors $\mathbf{e}_j$, $j = 1,2,3$, and a normalized "three-fold symmetry axis vector" obtained as the "trisector" [38]

$$\mathbf{e}_4 = \frac{\mathbf{q}_N}{|\mathbf{q}_N|} \tag{9}$$

with

$$\mathbf{q}_N = (\mathbf{e}_1 \times \mathbf{e}_2) + (\mathbf{e}_2 \times \mathbf{e}_3) + (\mathbf{e}_3 \times \mathbf{e}_1). \tag{10}$$

Since the E_a and E_b components of an E pair are connected by a rotation, a total of four symmetry-adapted functions $\bar{\alpha}_{A_1'}^{(1)}$, $\bar{\alpha}_{E_a'}^{(2a)}$, $\bar{\alpha}_{A_1'}^{(3)}$ and $\bar{\alpha}_{E_a'}^{(4a)}$ are required to describe the electronically averaged polarizability tensor of CH$_3$. These four functions are represented by polynomial expansions

$$\bar{\alpha}_\Gamma^{(k)}(\chi_1, \chi_2, \chi_3, \chi_{4a}, \chi_{4b}; \rho) = \alpha_0^{(\Gamma,k)}(\rho) + \sum_i \alpha_i^{(\Gamma,k)}(\rho) \chi_i$$
$$+ \sum_{i \leq j} \alpha_{ij}^{(\Gamma,k)}(\rho) \chi_i \chi_j + \sum_{i \leq j \leq k} \alpha_{ijk}^{(\Gamma,k)}(\rho) \chi_i \chi_j \chi_k \tag{11}$$
$$+ \sum_{i \leq j \leq k \leq l} \alpha_{ijkl}^{(\Gamma,k)}(\rho) \chi_i \chi_j \chi_k \chi_l,$$

in terms of the coordinates

$$\chi_k = \Delta r_k \exp \left[-(\Delta r_k)^2 \right], \quad (k = 1, 2, 3), \tag{12}$$

$$\chi_4 = (2\alpha_1 - \alpha_2 - \alpha_3)/\sqrt{6}, \tag{13}$$

$$\chi_5 = (\alpha_2 - \alpha_3)/\sqrt{2}, \tag{14}$$

where r_k denotes the C–H$_k$ bond length and α_1, α_2, and α_3 are three inter-bond angles $\angle(H_2$–C–$H_3)$, $\angle(H_1$–C–$H_3)$, and $\angle(H_1$–C–$H_2)$, respectively. The expansion coefficients $\alpha_{ij\dots}^{(\Gamma,k)}(\rho)$ are polynomials of the out-of-plane vibrational coordinate ρ (with the equilibrium value of 90°)

$$\alpha_{ij\dots}^{(\Gamma,k)}(\rho) = \sum_{s=0}^{N} \alpha_{ij\dots}^{\Gamma(k,s)} (1 - \sin \rho)^s, \tag{15}$$

where the maximal order of the polynomial is $N = 6$.

The expansion coefficients were determined in least-squares fittings to the 19 361 *ab initio* data points with root-mean-square deviations of 0.003 a.u. for all four components. The polarizability surface is given as supplementary data to this paper in the form of a Fortran 90 program and can be also accessed at ee Ref. 39.

2.3. Raman transitions

In the Placzek approximation [40], non-resonant Raman transition probabilities for a freely rotating molecule are obtained in terms of transition matrix elements of the polarizability tensor between the ro-vibrational wave functions of the initial and final transition states [8]. The Raman intensity for a gas-phase molecule in thermal equilibrium at the absolute temperature T can be expressed as the differential scattering cross section

$$\left[\frac{d\sigma_k}{d\Omega}(\nu_0) \right]_{\text{Stokes}} = \left(\frac{\pi}{\epsilon_0} \right)^2 \times (\nu_0 - \nu_k)^4 \times \frac{\exp(-E''/kT)}{Q_v}$$
$$\times \sum_{FF'} |\langle \Phi_{\text{rv}}' | \bar{\alpha}_{FF'} | \Phi_{\text{rv}}'' \rangle|^2. \tag{16}$$

Here, F and F' $(= X, Y, Z)$ signify axes of the space-fixed axis system [8], ϵ_0 is the vacuum permittivity, ν_0 is the frequency of the incident laser beam, ν_k is the frequency of the Raman-scattered radiation, Q_v is the vibrational partition function, $\langle \Phi_{\text{rv}}' | \bar{\alpha}_{FF'} | \Phi_{\text{rv}}'' \rangle$ is a transition matrix element of the electronically averaged polarizability tensor component $\bar{\alpha}_{FF'}$ between the two rovibrational wavefunctions Φ_{rv}'' and Φ_{rv}' of the initial and final states, respectively. Further, E'' is the energy of the initial state, k is the Boltzmann constant, and Ω is the solid angle within which the Raman-scattered light is detected.

It is well known that for absorption and emission, the 'readiness' of the molecule to undertake a transition from the initial state i (with ro-vibrational wavefunction Φ_{rv}'') to the final state f (with ro-vibrational wavefunction Φ_{rv}') is governed by the *line strength* [8, 41, 42]

$$S(f \leftarrow i) = g_{\text{ns}} \sum_{m', m''} \sum_{F=X,Y,Z} \left| \left\langle \Phi_{\text{rv}}' \left| \bar{\mu}_F \right| \Phi_{\text{rv}}'' \right\rangle \right|^2, \tag{17}$$

where g_{ns} is the nuclear spin statistical weight factor [8, 42] and $\bar{\mu}_F$ is the electronically averaged component of the molecular dipole moment along the space-fixed axis $F = X$, Y, or Z. The quantum numbers m' and m'' are the projections of the total angular momentum, in units of $\hbar$, on the Z axis in the initial and final states, respectively.

In the expression for the line strength Eq. (17) we sum the squares of the $\bar{\mu}_F$ matrix elements over all degeneracies of the initial and final states. Similarly, we sum the matrix element square in Eq. (16) to obtain a quantity measuring the readiness of the molecule to carry out a (nonresonant) Raman transition from state i to state f

$$\mathcal{R}(f \leftarrow i) = g_{\text{ns}} \sum_{m', m''} \sum_{F=X,Y,Z} \sum_{F'=X,Y,Z} |\langle \Phi_{\text{rv}}' | \bar{\alpha}_{FF'} | \Phi_{\text{rv}}'' \rangle|^2. \tag{18}$$

Equation (18) is converted to a form useful for the simulation of Raman spectra in a procedure very similar to that used for the line strength in Refs. [35, 41, 8, 42] (see also Refs. [43, 9, 44]). The first step in this procedure is to transform the space-fixed polarizability components $\bar{\alpha}_{FF'}$ to irreducible tensor [44] form

$$\bar{\alpha}_0^{(0,s)} = -\frac{1}{\sqrt{3}}[\bar{\alpha}_{XX} + \bar{\alpha}_{YY} + \bar{\alpha}_{ZZ}], \tag{19}$$

$$\bar{\alpha}_0^{(2,s)} = \frac{1}{\sqrt{6}}[2\bar{\alpha}_{ZZ} - \bar{\alpha}_{XX} - \bar{\alpha}_{YY}], \tag{20}$$

$$\bar{\alpha}_{\pm 1}^{(2,s)} = \frac{1}{2}\left[\mp(\bar{\alpha}_{XZ} + \bar{\alpha}_{ZX}) - i(\bar{\alpha}_{YZ} + \bar{\alpha}_{ZY})\right], \tag{21}$$

$$\bar{\alpha}_{\pm 2}^{(2,s)} = \frac{1}{2}\left[\bar{\alpha}_{XX} - \bar{\alpha}_{YY} \pm i(\bar{\alpha}_{XY} + \bar{\alpha}_{YX})\right]. \tag{22}$$

The molecule-fixed irreducible tensor components $\bar{\alpha}_{\sigma'}^{(\omega,m)}$ [ω = 0 or 2; $\sigma' = -\omega, -\omega + 1, \ldots, \omega$], defined in terms of the molecule-fixed axes xyz, are given by expressions obtained from Eqs. (19)–(22) by replacing (X, Y, Z) by (x, y, z). The space-fixed $\bar{\alpha}_\sigma^{(\omega,s)}$ components are related to their molecule-fixed counterparts $\bar{\alpha}_{\sigma'}^{(\omega,m)}$ as [8, 44]

$$\bar{\alpha}_\sigma^{(\omega,s)} = \sum_{\sigma'=-\omega}^{\omega} \bar{\alpha}_{\sigma'}^{(\omega,m)} D_{\sigma',\sigma}^{(\omega)*}(\theta, \phi, \chi) \tag{23}$$

where $D_{\sigma',\sigma}^{(\omega)}(\theta, \phi, \chi)$ is an element of a Wigner rotation matrix [44] and (θ, ϕ, χ) are the standard Euler angles[8, 42, 44] defining the orientation of the molecule-fixed axes xyz axes relative to the space-fixed axes XYZ axes.

In the TROVE approach [6, 7], the wavefunctions Φ''_{rv} and Φ'_{rv} are expressed as linear combinations of basis functions, i.e.,

$$|\Phi''_{rv}\rangle = \sum_{V''K''\tau''_{rot}} C''_{V''K''\tau''_{rot}} |J'' K'' m'' \tau''_{rot}\rangle |V''\rangle \tag{24}$$

with an analogous expression for Φ'_{rv}. In Eq. (24), the $C''_{V''K''\tau''_{rot}}$ are expansion coefficients, $|J'' K'' m'' \tau''_{rot}\rangle$ is a symmetrized rotational basis function, τ''_{rot} (= 0 or 1) determines the rotational parity as $(-1)^{\tau''_{rot}}$, and $|V''\rangle$ is a vibrational basis function. The TROVE basis functions $|J'' K'' m'' \tau''_{rot}\rangle |V''\rangle$ are explained in detail in Refs. [6, 7, 45].

In order to compute values of $\mathcal{R}(f \leftarrow i)$ in Eq. (18) we require the matrix elements $\langle \Phi'_{rv} | \bar{\alpha}_{FF'} | \Phi''_{rv}\rangle$. We can express these in terms of the irreducible-tensor matrix elements $\langle \Phi'_{rv} | \bar{\alpha}_\sigma^{(\omega,s)} | \Phi''_{rv}\rangle$ by means of Eqs. (19)–(22). We further obtain

$$\langle \Phi'_{rv} | \bar{\alpha}_\sigma^{(\omega,s)} | \Phi''_{rv}\rangle = \sum_{V'K'\tau'_{rot}} \sum_{V''K''\tau''_{rot}} \left(C'_{V'K'\tau'_{rot}}\right)^* C''_{V''K''\tau''_{rot}}$$
$$\times \sum_{\sigma'=-\omega}^{\omega} \langle J' K' m' \tau'_{rot} | D_{\sigma',\sigma}^{(\omega)*}(\theta, \phi, \chi) | J'' K'' m'' \tau''_{rot}\rangle$$
$$\times \langle V' | \bar{\alpha}_{\sigma'}^{(\omega,m)} | V''\rangle \tag{25}$$

by inserting Eqs. (23) and (24) (and the analogous expression for Φ'_{rv}) in the expression for $\langle \Phi'_{rv} | \bar{\alpha}_\sigma^{(\omega,s)} | \Phi''_{rv}\rangle$, and making use of the fact that $|J' K' m' \tau'_{rot}\rangle$, $D_{\sigma',\sigma}^{(\omega)*}$ and $|J'' K'' m'' \tau''_{rot}\rangle$ depend

solely on the Euler angles (θ, ϕ, χ), whereas $|V'\rangle$, $\bar{\alpha}_{\sigma'}^{(\omega,m)}$, and $|V''\rangle$ depend on the vibrational coordinates only.

Equation (25) is finally inserted in the expression for $\mathcal{R}(f \leftarrow i)$ [Eq. (18)] with the Euler-angle-dependent matrix element $\langle J' K' m' \tau'_{rot} | D_{\sigma',\sigma}^{(\omega)*}(\theta, \phi, \chi) | J'' K'' m'' \tau''_{rot}\rangle$ obtained analytically from Eq. (14-23) of Ref. [8], and the summations over m' and m'' carried out analytically by means of Eq. (14-32) of Ref. [8]. In this manner, we determine a detailed expression for $\mathcal{R}(f \leftarrow i)$ that is highly analogous to the expression for $S(f \leftarrow i)$ given, for example, in Eq. (21) of Ref. [41].

Whereas the expression for the absorption and emission line strength in Eq. (17) is obtained in terms of irreducible tensor elements with $\omega = 1$ only, that is with one ω-value, the expression for $\mathcal{R}(f \leftarrow i)$ involves two ω-values, $\omega = 0$ and 2. We denote the corresponding contributions to $\mathcal{R}(f \leftarrow i)$ as $\mathcal{R}_0(f \leftarrow i)$ and $\mathcal{R}_2(f \leftarrow i)$, respectively, by analogy to the quantities $R_0(f \leftarrow i)$ and $R_2(f \leftarrow i)$ defined in Eqs. (14-132) and (14-133) of Ref. [8]. In conventional Raman-spectroscopy parlance, $\mathcal{R}_0(f \leftarrow i)$ accounts for the intensity resulting from *isotropic* Raman scattering, while $\mathcal{R}_2(f \leftarrow i)$ is the contribution from *anisotropic* Raman scattering.

The quantities $\mathcal{R}_0(f \leftarrow i)$ and $\mathcal{R}_2(f \leftarrow i)$ depend on the vibrational matrix elements $\langle V' | \bar{\alpha}_{\sigma'}^{(\omega,m)} | V''\rangle$. These are calculated by first expressing the molecule-fixed irreducible tensor operator $\bar{\alpha}_{\sigma'}^{(\omega,m)}$ in terms of Cartesian components $\bar{\alpha}_{\alpha\beta}$ $(\alpha, \beta = x, y, z)$, see Eqs. (19)-(22) where the X, Y, and Z are replaced by x, y, and z. The functions $\bar{\alpha}_{\alpha\beta}$ are obtained in the electronic structure calculations and represented by polynomials of internal molecular coordinates, as explained above in the Section 2.2, and the vibrational matrix elements are calculated similarly to those of the vibrational Hamiltonian and the dipole moment.

The contributions to $\mathcal{R}(f \leftarrow i)$ from $\mathcal{R}_0(f \leftarrow i)$ and $\mathcal{R}_2(f \leftarrow i)$ depend on the experimental set-up (see, for example, Eqs. (14-134) and (14-135) of Ref. [8]). We consider here the case of perpendicular Raman scattering assuming the laser light is polarized in the Y direction and the exciting laser beam is propagating in the X direction. In this situation, the differential Raman scattering cross section for a rovibrational transition is

$$\left[\frac{d\sigma_k}{d\Omega}(\nu_0)\right]_{\text{Stokes}} = \left(\frac{\pi}{\epsilon_0}\right)^2 \times (\nu_0 - \nu_k)^4 \times \frac{\exp(-E''/kT)}{Q_v}$$
$$\times \left[|\langle \Phi'_{rv} | \bar{\alpha}_{YY} | \Phi''_{rv}\rangle|^2 + |\langle \Phi'_{rv} | \bar{\alpha}_{YX} | \Phi''_{rv}\rangle|^2\right]. \tag{26}$$

It can be shown that in terms of $\mathcal{R}_0(f \leftarrow i)$ and $\mathcal{R}_2(f \leftarrow i)$, Eq. (26) yields

$$\left[\frac{d\sigma_k}{d\Omega}(\nu_0)\right]_{\text{Stokes}} = \left(\frac{\pi}{\epsilon_0}\right)^2 \times (\nu_0 - \nu_k)^4 \times \frac{\exp(-E''/kT)}{Q_v}$$
$$\times \frac{1}{30}\left(10\,\mathcal{R}_0(f \leftarrow i) + 7\,\mathcal{R}_2(f \leftarrow i)\right). \tag{27}$$

Our complete Raman line list for CH_3 can be accessed via the Zenodo repository www.zenodo.org, see Ref. 39.

3. Results, Summary, and Discussion

Table 1: Comparison of experimental and theoretical term values (cm^{-1}) for selected ^{12}CH$_3$ levels.

State	Γ^a	Obs.^{b}	Ref.^{c}	Calc.^{d}
ν_1	A'_1	3004.42	[27]	3002.76
ν_2	A''_2	606.45	[57]	602.43
$2\nu_2$	A'_1	1288.1	[57]	1281.24
ν_3	E'	3160.8	[58]	3158.83
ν_4	E'	1397.0	[59]	1387.26

^{a} $\boldsymbol{D}_{3h}$(M) symmetry of the vibrational state.

^{b} Experimental term value.

^{c} Reference for experimental term value.

^{d} Variationally computed value from Ref. [1]; TROVE calculation with basis set $P_{max} = 32$ [1].

3.1. Results

The methyl radical has four vibrational normal modes: the symmetric stretch, $\nu_1(A'_1)$, the out-of-plane bending, $\nu_2(A''_2)$, the degenerate asymmetric stretch, $\nu_3(E')$, and the degenerate in-plane bending, $\nu_4(E')$. For each normal mode, we give in parentheses its symmetry in the molecular symmetry group $\boldsymbol{D}_{3h}$(M) (see Table A-10 of Ref. [8]). The fundamental band associated with the ν_1 mode, of A'_1 symmetry, is detectable as Raman transition only; it is forbidden in absorption and emission. The ν_2 fundamental transition is neither infrared nor Raman active. The fundamental transitions involving the E'-symmetry modes ν_3 and ν_4 are allowed both as IR and Raman transitions. We study here the symmetric C-H stretch mode, $\nu_1(A'_1)$, of CH$_3$ in the electronic ground state. The experimental value of the ν_1-band origin has been determined as 3002.4 cm^{-1} from resonance-Raman spectra [46] and as 3004.8 and 3004.4 cm^{-1}, respectively, in two CARS experiments [26, 27]. Further CARS studies [47, 48] have produced similar values. From harmonic force-field analysis an estimation of 3044 cm^{-1} has been reported [49] for the ν_1 fundamental term value; this value is corrected to 2992.6 cm^{-1} when anharmonic corrections are taken into account [50]. Several calculations of the ν_1 term value have been reported using *ab initio* methods [51, 52, 53, 54] and methods considering vibrational nuclear motion only [55, 56]. The best prediction was 3002.0 cm^{-1} from a vibrational many-body method, the vibrational configuration interaction (VCI) method [54]. Our computational work has produced [1] a value of 3002.8 cm^{-1}. In Table 1, we compare the available, experimentally derived term values for ^{12}CH$_3$ with the calculated values from Ref. [1]; the calculations of the present work involve the same calculated values. It is seen that our calculations reproduce the experimental results to better than 1%. Predicted term values for other vibrational states are given in Table 1 of Ref. [1].

To simulate the nonresonant Raman spectrum for the methyl radical, we have computed the differential Raman scattering cross sections [Eq. (26)] for the CH$_3$ Raman transitions between 0 and 6000 cm^{-1} allowed by the selection rules given
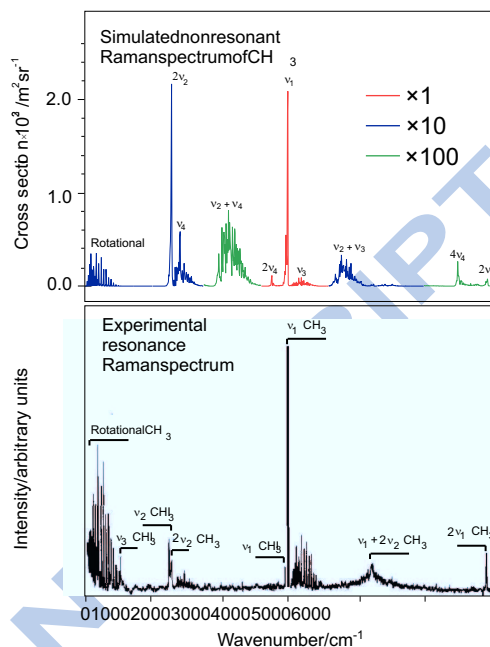

Figure 1: A comparison between the simulated nonresonant (at $T = 300$ K) and an observed resonance Raman spectrum of CH$_3$ (see text). In the simulated nonresonant Raman spectrum of CH$_3$ (top display), the ordinate is multiplied by 1, 10, and 100, respectively, in the red, blue, and green parts of the curve. The assignments of the bands given are those suggested by analysis of the TROVE wavefunctions. The experimental resonance Raman spectrum (bottom display) contains transitions of CH$_3$ and CH$_3$I; it is reproduced from Fig. 1 of Ref. [46] by permission from Elsevier. The assignments of the bands given are from Ref. [46].

in Section 14.3 of Ref. [8]: $|J' - J''| \leqslant \omega$, $J' + J'' \geqslant \omega$, and $\Gamma''_{rv} = \Gamma'_{rv}$, where Γ''_{rv} and Γ'_{rv} are the molecular-symmetry-group symmetries of the initial and final states, respectively. The top display of Fig. 1 presents an overview of the computed Raman spectrum as cross-sections (in units of m^2/sr) of CH$_3$ at room temperature. In the figure, this spectrum is compared to the experimental resonance Raman spectrum[1] from Ref. [46]. Figure 2 shows a similar comparison to the CARS spectrum of the ν_1 Q branch[2] from Ref. [26]. In this figure we show the individual contributions from $\mathcal{R}_0$ and $\mathcal{R}_2$ from Eq. (27), before averaging with the Placzek coefficients 10/30 and 7/10. Consistently with the band center theory-experimental deviation in Table 1, the theoretical spectrum is shifted by about 1.5 cm^{-1} relative to the experimental one.

3.2. Summary and Discussion

In the present work, we have extended the TROVE [24, 25] program so as to allow the simulation of nonresonant Raman

---

[1]Reprinted from Chemical Physics Letters, Vol. 151, P.B. Kelly and Sjon G. Westre, Resonance Raman Spectroscopy of the Methyl Radical, pp. 253–257, Copyright 1968, with permission from Elsevier.

[2]Reprinted from the Journal of Chemical Physics, Vol. 81, P. L. Holt, K. E. McCurdy, R. B. Weisman, J. S. Adams, P. S. Engel, Transient CARS spectroscopy of the ν_1 band of methyl radical, pp. 3349–3350, Copyright 1984, with permission from AIP Publishing.
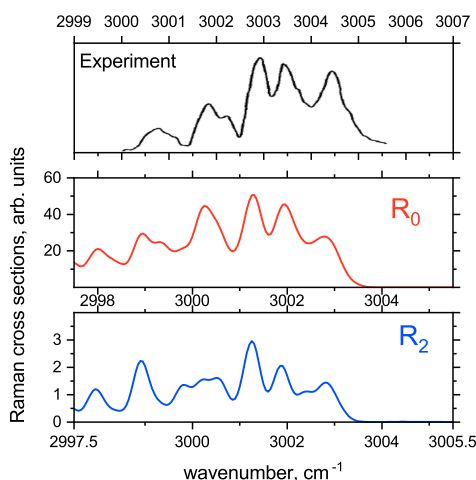
Figure 2: A comparison between the simulated nonresonant Raman spectrum (at T = 300 K) and an observed CARS spectrum of the ν_1 band Q branch of CH_3 (top display). It is reproduced from Fig. 1 of Ref. [26] by permission from AIP Publishing. We show the simulated, individual contributions from $\mathcal{R}_0$ and $\mathcal{R}_2$, before applying the Placzek coefficients of 10/30 and 7/10. The simulated spectra were convolved with a Gaussian line profile with a half-width-at-half-maximum of 0.2 cm^{-1}. Note that the theoretical spectra are shifted by about 1.5 cm^{-1} relative to the experimental CARS spectrum to account for the obs−calc difference for the ν_1 band center (Table 1).

spectra. The corresponding simulations take into account the complete rovibrational nuclear motion, using the fully-coupled TROVE [24, 25] rovibrational wavefunctions. We have applied the new program module for simulating the nonresonant Raman spectrum of the methyl radical CH_3; the simulations are based on potential energy and polarizability surfaces calculated *ab initio* for the electronic ground state of CH_3 with the MOL-PRO [31] program package at the ROHF-RCCSD(T)/aug-cc-pVTZ level of theory.

Fig. 1 includes the nonresonant Raman spectrum simulated in the present work. Comparing the simulated spectrum to an experimental counterpart is not currently possible because to the best of our knowledge, no such spectrum is available in the literature. However, a resonance Raman spectrum of CH_3 has been published [46] and we include also this spectrum in Fig. 1 with the band assignments from Ref. [46].

The difference between nonresonant Raman spectra and their RR counterparts is explained above; in the RR case the intensities of some Raman transitions are greatly enhanced. The comparison of the simulated non-resonant Raman spectrum to the published RR one [46] is, of course, somewhat problematic. However, both spectra contain the same Raman transitions, just with different (absolute and relative) intensities. So we recognize that the strongest vibrational Raman transition, the ν_1 fundamental band observed experimentally at 3004.4 cm^{-1}, is clearly present in both spectra. So is the first overtone band $2\nu_2$ (predicted at 1288.09 cm^{-1}). For the ν_1 and $2\nu_2$ bands, rotational structure is recognizable in both experimental and simulated spectra. Similarly, the nonresonant Raman spectrum con-

tains the same transitions as the CARS one, and we see in Fig. 2 that our simulation of the linear, nonresonant Raman spectrum of the Q branch in the ν_1 band of CH_3 reproduces rather well the salient features of the experimental, nonlinear CARS spectrum.

The two fundamental modes ν_3 (at 3160.8 cm^{-1}) and ν_4 (at 1397.0 cm^{-1}) are Raman active but they are not assigned in the resonance Raman experiment. However, around both wavenumber values there is weak, but visible rotational structure in the experimental resonance Raman spectrum, possibly caused by these bands. Above 3160.8 cm^{-1}, the position of the ν_3 band, there are two bands noticeable in the experimental resonance Raman of Fig. 1, whereas three bands are present in the simulated spectrum. The two bands in the experimental spectrum are assigned as $\nu_1 + 2\nu_2$ and $2\nu_1$, respectively, while TROVE suggests the labelling $\nu_2 + \nu_3$, $4\nu_4$, and $2\nu_1$ for the three bands visible in the simulation. It is conceivable, however, that the resonance Raman technique favors other vibrational transitions that nonresonant Raman, so possibly the significant bands must be assigned differently in the two spectra.

As mentioned above, CH_3 belongs to the $\boldsymbol{D}_{3h}(M)$ molecular symmetry group and its equilibrium structure has $\boldsymbol{D}_{3h}$ point group symmetry [8]. Consequently, the absorption/emission transitions in the pure rotational spectrum and in the ν_1 fundamental band involve intensity borrowing [8] so that their observation is extremely difficult and probably impossible at the present time. It is nevertheless important to obtain experimental information on the ν_1 band, for example in connection with studies of the energy distribution in methyl halide photodissociation dynamics. Such information can be obtained from Raman spectroscopy which in many cases complements absorption/emission. With the extension of the TROVE [24, 25] program reported in the present work, we can simulate nonresonant Raman spectra and thus assist the recording and interpretation of laboratory Raman spectra.

Acknowledgments

SUPPLEMENTARY MATERIAL

See supplementary material for Fortran 90 source code files, and the associated parameter input files, for computing the electric polarizability tensor of CH_3. The complete Raman line list for CH_3, together with the supplementary material just mentioned, can be accessed at the Zenodo repository [39].

REFERENCES

[1] A. Y. Adam, A. Yachmenev, S. N. Yurchenko, P. Jensen, A Variationally Computed IR Line List for the Methyl Radical CH_3, The Journal of Phys-

ical Chemistry A, in press.
URL https://doi.org/10.1021/acs.jpca.9b02919

[2] A. Y. Adam, A. Yachmenev, S. N. Yurchenko, P. Jensen, Ro-vibrational averaging of the isotropic hyperfine coupling constant for the methyl radical, J. Chem. Phys. 143 (2015) 244306/1–7.

[3] G. D. Stancu, J. Röpcke, P. B. Davies, Line strengths and transition dipole moment of the ν_2 fundamental band of the methyl radical, J. Chem. Phys. 122 (2005) 014306/1–11.

[4] A. G. Császár, C. Fábri, T. Szidarovszky, E. Mátyus, T. Furtenbacher, G. Czakó, The fourth age of quantum chemistry: molecules in motion, Phys. Chem. Chem. Phys. 14 (2012) 1085–1106.

[5] L. Lodi, J. Tennyson, Theoretical methods for small-molecule ro-vibrational spectroscopy, J. Phys. B: At. Mol. Opt. Phys. 43 (2010) 133001/1–44.

[6] J. Tennyson, S. N. Yurchenko, ExoMol: molecular line lists for exoplanet and other atmospheres, Monthly Notices of the Royal Astronomical Society 425 (2012) 21–33.

[7] J. Tennyson, S. N. Yurchenko, A. F. Al-Refaie, E. J. Barton, K. L. Chubb, P. A. Coles, S. Diamantopoulou, M. N. Gorman, C. Hill, A. Z. Lam, L. Lodi, L. K. McKemmish, Y. Na, A. Owens, O. L. Polyansky, T. Rivlin, C. Sousa-Silva, D. S. Underwood, A. Yachmenev, E. Zak, The ExoMol database: molecular line lists for exoplanet and other hot atmospheres, J. Mol. Spectrosc. 327 (2016) 73–94.

[8] P. R. Bunker, P. Jensen, Molecular Symmetry and Spectroscopy, 2nd Edition, NRC Research Press, Ottawa, 1998.

[9] F. Hegelund, F. Rasmussen, S. Brodersen, The Selection Rules and the Transition Moment for Rotation-Vibrational Transitions in Axial Molecules, J. Raman Spectrosc. 1 (1973) 433–453.

[10] J. M. Fernández, G. Tejeda, M. Carvajal, M. L. Senent, New spectral characterization of dimethyl ether isotopologues CH_3OCH_3 and $^{13}CH_3OCH_3$ in the THz region, The Astrophysical Journal Supplement Series 241 (2019) 13/1–9.

[11] R. Lemus, M. Sánchez-Castellanos, F. Pérez-Bernal, J. M. Fernández, M. Carvajal, Simulation of the Raman spectra of CO_2: Bridging the gap between algebraic models and experimental spectra, J. Chem. Phys. 141 (2014) 054306/1–14.

[12] J. F. Verdieck, S. H. Peterson, C. M. Savage, P. D. Maker, Hyper-Raman Spectra of Methane, Ethane, and Ethylene in Gas Phase, Chem. Phys. Lett. 7 (1970) 219–222.

[13] M. Ringholm, R. Bast, L. Oggioni, U. Ekström, K. Ruud, Analytic calculations of hyper-Raman spectra from density functional theory hyperpolarizability gradients, J. Chem. Phys. 141 (2014) 134107/1–10.

[14] L. Maschio, B. Kirtman, M. Rérat, R. Orlando, R. Dovesi, Ab initio analytical Raman intensities for periodic systems through a coupled perturbed Hartree-Fock/Kohn-Sham method in an atomic orbital basis. I. Theory, J. Chem. Phys. 139 (2013) 164101/1–13.

[15] L. Jensen, C. M. Aikens, G. C. Schatz, Electronic structure methods for studying surface-enhanced Raman scattering, Chem. Soc. Rev. 37 (2008) 1061–1073.

[16] C. V. Raman, A New Radiation, Indian J. Phys. 2 (1928) 387–398.

[17] G. Landsberg, L. Mandelstam, Eine neue Erscheinung bei der Lichtzerstreuung in Krystallen, Naturwissenschaften 16 (1928) 557–558.

[18] A. Smekal, Zur Quantentheorie der Dispersion, Naturwissenschaften 11 (1923) 873–875.

[19] R. J. H. Clark, P. D. Mitchell, Resonance Raman and Preresonance Raman Spectra of Titanium Tetraiodide, J. Amer. Chem. Soc. 95 (1973) 8300–.

[20] D. Rappoport, S. Shim, A. Aspuru-Guzik, Simplified sum-over-states approach for predicting resonance Raman spectra. Application to nucleic acid bases, J. Phys. Chem. Lett. 2 (2011) 1254–1260.

[21] J. Guthmuller, Assessment of TD-DFT and CC2 methods for the calculation of resonance Raman intensities: Application to o-nitrophenol, J. Chem. Theory Comput. 7 (2011) 1082–1089.

[22] D. W. Silverstein, N. Govind, H. J. J. van Dam, L. Jensen, Simulating One-Photon Absorption and Resonance Raman Scattering Spectra Using Analytical Excited State Energy Gradients within Time-Dependent Density Functional Theory, J. Chem. Theory Comput. 9 (2013) 5490–5503.

[23] A. Baiardi, J. Bloino, V. Barone, Accurate Simulation of Resonance-Raman Spectra of Flexible Molecules: An Internal Coordinates Approach, J. Chem. Theory Comput. 11 (2015) 3267–3280.

[24] S. N. Yurchenko, W. Thiel, P. Jensen, Theoretical ROVibrational Energies (TROVE): A robust numerical approach to the calculation of rovibrational

energies for polyatomic molecules, J. Mol. Spectrosc. 245 (2007) 126–140.

[25] A. Yachmenev, S. N. Yurchenko, Automatic differentiation method for numerical construction of the rotational-vibrational Hamiltonian as a power series in the curvilinear internal coordinates using the Eckart frame, J. Chem. Phys. 143 (2015) 014105/1–16.

[26] P. L. Holt, K. E. McCurdy, R. B. Weisman, J. S. Adams, P. S. Engel, Transient CARS spectroscopy of the ν_1 band of methyl radical, J. Chem. Phys. 81 (1984) 3349–3350.

[27] N. E. Triggs, M. Zahedi, J. W. Nibler, P. DeBarber, J. J. Valentini, High resolution study of the ν_1 vibration of CH_3 by coherent Raman photofragment spectroscopy, J. Chem. Phys. 96 (1992) 1822–1831.

[28] G. Knizia, T. B. Adler, H.-J. Werner, Simplified CCSD(t)-f12 methods: Theory and benchmarks, J. Chem. Phys. 130 (2009) 054104/1–20.

[29] K. A. Peterson, T. B. Adler, H.-J. Werner, Systematically convergent basis sets for explicitly correlated wavefunctions: The atoms H, He, B-Ne, and Al-Ar, J. Chem. Phys. 128 (2008) 084102/1–12.

[30] H. Lin, W. Thiel, S. N. Yurchenko, M. Carvajal, P. Jensen, Vibrational energies for NH_3 based on high level ab initio potential energy surfaces, J. Chem. Phys. 117 (2002) 11265–11276.

[31] H. J. Werner, P. J. Knowles, G. Knizia, F. R. Manby, M. Schütz, Molpro: A general-purpose quantum chemistry program package, Wiley Interdisciplinary Reviews: Computational Molecular Science 2 (2012) 242–253.

[32] J. D. Watts, J. Gauss, R. J. Bartlett, Coupled-cluster methods with noniterative triple excitations for restricted open-shell hartree–fock and other general single determinant reference functions. energies and analytical gradients, J. Chem. Phys. 98 (1993) 8718–8733.

[33] T. H. Dunning, Gaussian basis sets for use in correlated molecular calculations. I. The atoms boron through neon and hydrogen, J. Chem. Phys. 90 (1989) 1007–1023.

[34] R. A. Kendall, T. H. Dunning, Jr., R. J. Harrison, Electron affinities of the first-row atoms revisited. Systematic basis sets and wave functions, J. Chem. Phys. 96 (1992) 6796–6806.

[35] S. N. Yurchenko, R. J. Barber, A. Yachmenev, W. Thiel, P. Jensen, J. Tennyson, A Variationally computed T=300 K line list for NH_3, J. Phys. Chem. A 113 (2009) 11845–11855.

[36] A. Yachmenev, J. Küpper, Communication: General variational approach to nuclear-quadrupole coupling in rovibrational spectra of polyatomic molecules, J. Chem. Phys. 147 (2017) 141101/1–6.

[37] A. Owens, A. Yachmenev, RichMol: A general variational approach for rovibrational molecular dynamics inxexternal electric fields, J. Chem. Phys. 148 (2018) 124102/1–9.

[38] S. N. Yurchenko, W. Thiel, M. Carvajal, P. Jensen, Ab initio potential energy surface, electric-dipole moment, polarizability tensor, and theoretical rovibrational spectra in the electronic ground state of $^{14}NH_3^+$, Chem. Phys. 346 (2008) 146–159.

[39] A. Y. Adam, P. Jensen, A. Yachmenev, S. N. Yurchenko, Supplementary material: Non-resonant Raman spectra of the methyl radical $^{12}CH_3$ simulated in variational calculations, Zenodo. https://doi.org/10.5281/zenodo.2607836 (Mar 2019).

[40] G. Placzek, Rayleigh-Streuung und Raman-Effekt, in: E. Marx (Ed.), Handbuch der Radiologie, Vol. 6, Academische Verlag, Leipzig, 1934, pp. 205–374.

[41] S. N. Yurchenko, W. Thiel, M. Carvajal, H. Lin, P. Jensen, Rotation-Vibration Motion of Pyramidal XY3 Molecules Described in the Eckart Frame: The Calculation of Intensities with Application to NH_3, Adv. Quantum Chem. 48 (2005) 209–238.

[42] P. R. Bunker, P. Jensen, The Fundamentals of Molecular Symmetry, 1st Edition, CRC Press, Boca Raton, 2004.

[43] F. Rasmussen, S. Brodersen, The Rotational Structure of Vibrational Bands of Symmetric Top Molecules, J. Mol. Spectrosc. 25 (1968) 166–173.

[44] R. N. Zare, Angular Momentum: Understanding Spatial Aspects in Chemistry and Physics, John Wiley and Sons, New York, 1988.

[45] S. N. Yurchenko, A. Yachmenev, R. I. Ovsyannikov, Symmetry-Adapted Ro-vibrational Basis Functions for Variational Nuclear Motion Calculations: TROVE Approach, J. Chem. Theory Comput. 13 (2017) 4368–4381.

[46] P. B. Kelly, S. G. Westre, Resonance Raman spectroscopy of the methyl radical, Chem. Phys. Lett. 151 (1988) 253–257.

[47] M. Zahedi, J. A. Harrison, J. W. Nibler, 266 nm CH_3I photodissocia-

8

tion: CH_3 spectra and population distributions by coherent Raman spectroscopy, J. Chem. Phys. 100 (1994) 4043–4055.

[48] S. Hädrich, S. Hefter, B. Pfelzer, T. Doerk, P. Jauernik, J. Uhlenbusch, Determination of the absolute Raman cross section of methyl, Chem. Phys. Lett. 256 (1996) 83–86.

[49] A. Snelson, Infrared matrix isolation spectrum of the methyl radical produced by pyrolysis of methyl iodide and dimethyl mercury, J. Phys. Chem. 74 (1970) 537–544.

[50] V. Špirko, P. R. Bunker, The potential function and rotation-vibration energy levels of the methyl radical CH_3, J. Mol. Spectrosc. 95 (1982) 381–390.

[51] D. M. Chipman, Theoretical study of the properties of methyl radical, J. Chem. Phys. 78 (1983) 3112–3132.

[52] P. Botschwina, J. Flesch, W. Meyer, Spectroscopic properties of the methyl radical calculated from UHF SCEP wavefunctions, Chem. Phys. 74 (1983) 321–338.

[53] J. Pacansky, W. Koch, M. D. Miller, Analysis of the Structures, Infrared Spectra, and Raman Spectra for the Methyl, Ethyl, Isopropyl, and tert-Butyl Radicals, J. Am. Chem. Soc. 113 (1991) 317–328.

[54] M. Keceli, T. Shiozaki, K. Yagi, S. Hirata, Anharmonic vibrational frequencies and vibrationally-averaged structures of key species in hydrocarbon combustion: HCO^+, HCO, HNO, HOO, HOO^-, CH_3^+, and CH_3, Mol. Phys. 107 (2009) 1283–1301.

[55] D. W. Schwenke, A theoretical study of the ro-vibrational spectrum of the X state of CH_3, Spectrochim. Acta A 55 (1999) 731–738.

[56] D. M. Medvedev, L. B. Harding, S. K. Gray, Methyl radical: Ab initio global potential surface, vibrational levels and partition function, Mol. Phys. 104 (2006) 73–81.

[57] C. Yamada, E. Hirota, K. Kawaguchi, Diode Laser Study of the ν_2 Band of the Methyl Radical, J. Chem. Phys. 75 (1981) 5256–5264.

[58] S. Davis, D. T. Anderson, G. Duxbury, D. J. Nesbitt, Jet-Cooled Molecular Radicals in Slit Supersonic Discharges: Sub-Doppler Infrared Studies of Methyl Radical, J. Chem. Phys. 107 (1997) 5661–5675.

[59] M. E. Jacox, Vibrational and Electronic Energy Levels of Polyatomic Transient Molecules. Supplement B, Vol. 1, American Chemical Society, New York, 2005.

Nonresonant Raman spectra of the methyl radical $^{12}CH_3$ simulated in variational calculations
by Ahmad Y. Adam, Per Jensen, Andrey Yachmenev, and Sergei N. Yurchenko.

HIGHLIGHTS

- The program TROVE computes variationally rovibrational states of smaller molecules.

- We have extended it to simulate nonresonant Raman spectra.

- Input for the simulations are *ab initio* potential and polarizability surfaces.

- Simulations for CH_3 are in good agreement with available experimental data.

- The extended program provides new support for remote-sensing experiments,

a

Simulated nonresonant Raman spectrum of CH_3